红外与激光工程
INFRARED AND LASER ENGINEERING
EI, SCOPUS, CSCD等收录期刊

纳秒脉冲激光诱导的金属膜喷发的分布特征

马彬　韩佳岐　王可　黄秋实　焦宏飞　管爽

Distribution characteristics of metal film eruption induced by nanosecond pulse laser

Ma Bin, Han Jiaqi, Wang Ke, Huang Qiushi, Jiao Hongfei, Guan Shuang

在线阅读 View online: https://doi.org/10.3788/IRLA20210036

Distribution characteristics of metal film eruption induced by nanosecond pulse laser

Ma Bin[1,2], Han Jiaqi[1,2], Wang Ke[1,2], Huang Qiushi[1,2], Jiao Hongfei[1,2], Guan Shuang[1,2]

(1. Institute of Precision Optical Engineering, School of Physical Science and Engineering, Tongji University, Shanghai 200092, China;
2. Key Laboratory of Advanced Micro-Structure Materials, Ministry of Education, Shanghai 200092, China)

Abstract: Thermo-mechanical damage occurs when a metal film layer is irradiated by a high-power nanosecond pulse laser. High temperature and high pressure induce the thermal evaporation of the metal film layer and particles outward ejection. Most of the ejected particles are in atomic and ionic states. In the energy dispersive spectroscopy analysis test, multiple sets of standard samples for comparison experiments was used to calibrate the test results in this paper, and an estimated method was given to calculate the number of deposited atoms based on the results. The differences of the eruption of Al film under different vacuum environments and atmospheric environments irradiated by different laser fluences were compared. And the eruption and spatial distribution characteristics of metal films with different melting points were compared. The experimental results were further analyzed and explained by combining the transient images captured by pump-probe technology.

Key words: nanosecond pulse laser; metal film; vacuum; evaporation and ejection of materials
CLC number: O437 **Document code:** A **DOI:** 10.3788/IRLA20210036

纳秒脉冲激光诱导的金属膜喷发的分布特征

马 彬[1,2], 韩佳岐[1,2], 王 可[1,2], 黄秋实[1,2], 焦宏飞[1,2], 管 爽[1,2]

(1. 同济大学 物理科学与工程学院 精密光学工程技术研究所, 上海 200092;
2. 先进微结构材料教育部重点实验室, 上海 200092)

摘 要: 大功率纳秒脉冲激光辐照金属膜层时会发生热力损伤,产生的高温和高压会引起金属膜层的热蒸发,从而向外喷射颗粒,大多数喷射粒子处于原子和离子状态。在能量色散光谱分析测试中,文中使用多组标准样品进行比较实验,校准测试结果,并给出了一种根据结果计算沉积原子数的估计方法。此外,在此基础上比较了不同真空度的真空环境和大气环境下铝膜喷发的差异,并且对比了不同熔点的金属膜的喷发及空间分布特征。通过结合泵探测技术捕获的瞬态图像,进一步分析和解释了实验结果。

关键词: 纳秒脉冲激光; 金属膜; 真空; 材料喷射蒸发

收稿日期:2021-01-13; **修订日期:**2021-03-15

基金项目:国家自然科学基金 (61675156, 61975153)

作者简介:马彬, 男, 教授, 博士生导师, 博士, 主要从事激光与物质相互作用及光学元件的精密检测方面的研究。

0 Introduction

The ejected particles or vaporized metal atoms caused by laser-induced optical elements damage are actively injected into the central high-temperature plasma region of the Tokamak device. From this step, we can infer the plasma disturbance and intensity distribution and analyze the correlation between the injected particles and plasma[1−2]. The interaction between nanosecond pulse laser and metal film layer is primarily the thermal-mechanical effect[3−5], which is closely related to thermal absorption, diffusion, and conduction. When a high-power laser induces damage in a metal film, the strong absorption will increase the temperature and pressure in the partial film layer, and the plasma ball will form and constantly extend and expand. The thermal effect and stress increase as the temperature and pressure increase gradually until the effect and stress exceed the tensile strength of the material[6]. Finally, the metal film layer is fractured, melted, and evaporated. This process is called laser-induced damage or laser ablation[7−8]. A large number of studies show that the degree of laser ablation is related to laser wavelength, pulse width, and properties of the material (i.e., absorption rate, thermal diffusion, melting point, and boiling point)[9−13].

During eruption, a small portion of the metal film peels off and is jolted by a reverse force to start flying outwards, which is similar to the ejection of particles[14−16]. However, the metal film layer is mainly ejected in the evaporative state, the evaporated atoms and a small number of layers of peeling block films are depleted during ejection. Thus, the received or injected number of particles is a crucial factor to consider in studying the plasma status in Tokamak and the process of thermal evaporation eruption[2].

Energy Dispersive Spectroscopy (EDS) is used to evaluate the information on deposited atoms by detecting the relevant elements and obtaining the relative atomic ratio and quality ratio of different elements[17]. Given the lack of the electron beam detection depth, specific X-ray escape ability of metal atoms at different depths, and total number of detected atoms collected in the test area, calculating the number of metal element atoms via the EDS method is impossible. Although pulsed laser deposition technology is more concerned with depositional efficiency and state, the deposition effect can be estimated by pulsed laser only when the film layer has a certain thickness and quality differences with long-term cumulative effects[18]. Consequently, obtaining information on the eruption and deposition of particles of the metal film layer under the action of a single pulse laser is difficult.

In this paper, we aim to develop an estimated method for calculating the number of particles ejected from a metal film layer irradiated by a single pulsed laser. By preparing a series of standard samples and calibrating the EDS detection depth, information on the escape intensity of specific signals of metal elements at different depths is obtained. Moreover, the amount of metal elements deposited on the external receiving plate is estimated. By using pump-probe imaging technology, the transient eruption characteristics of metal films are captured, the differences between the vacuum and atmospheric environments are evaluated. On the basis of the deposited atomic ratio of different experimental conditions, the factors influencing metal eruption are analyzed.

1 Experimental setup

As shown in Fig.1(a), the Laser-Induced Damage Threshold (LIDT) measurement system that includes pump-probe imaging technology is used. The 1 064 nm wavelength laser with 10 ns pulse width is used as the pump laser, whereas the 532 nm wavelength laser with 8.5 ns pulse width is used as the probe laser. The transient process of metal film ejection at different times is captured by adjusting the length of the relative path of the two beams. Using a lens with a focal length of 300 mm, the spot diameter is determined to be approximately 0.1 mm. The particle receiving plate is placed behind 25 mm of the sample; information on the submicron-sized

particles is monitored by an online microscope. The atomic-state metal elements formed by thermal evaporation are deposited on the receiving plate, and the distribution of the elements is measured by EDS. Figure 1(b) shows the small vacuum devices employed to obtain a low vacuum degree of about 100 Pa by using a mechanical pump. Thus, the differences in the characteristics of metal film eruptions under vacuum and atmospheric environments can be compared and analyzed.

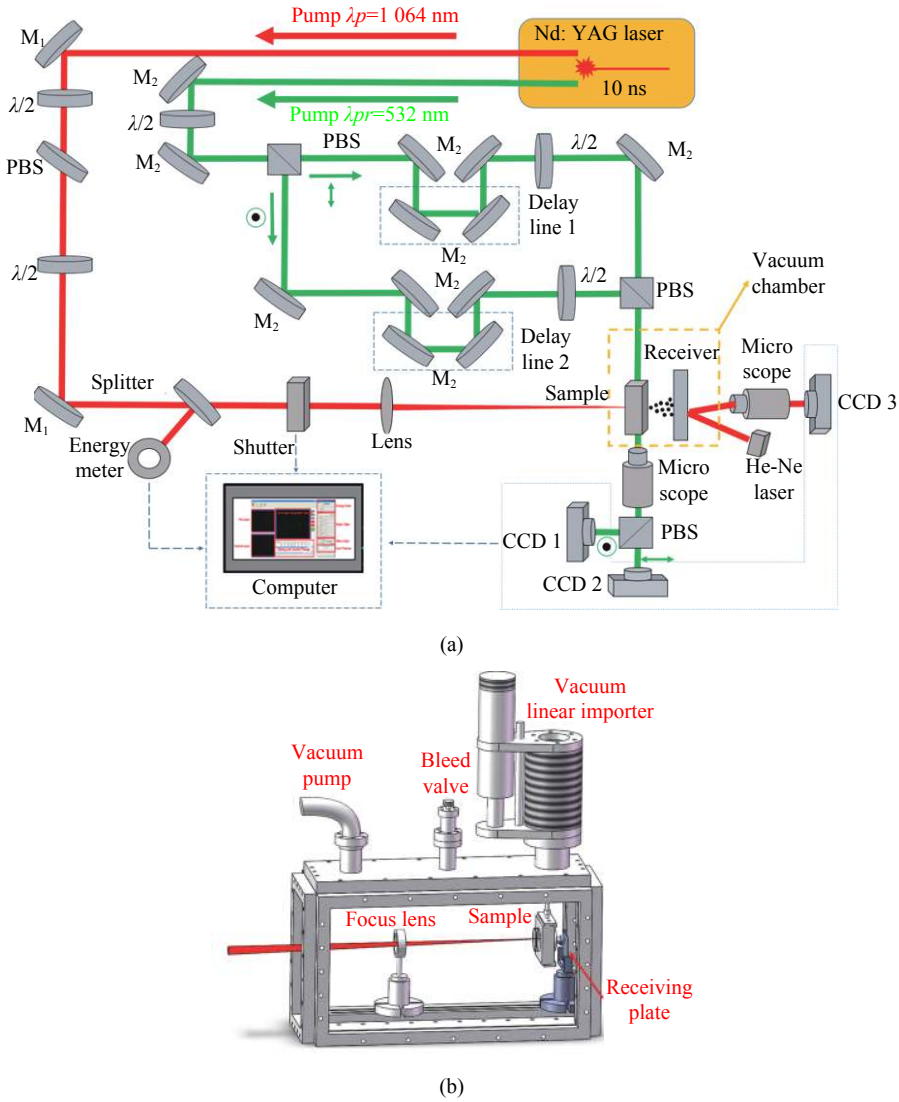

Fig.1 Schematic of experimental equipment. (a) LIDT test system with pump-probe technology; (b) A small vacuum system

2 Evaporation model of metal film

2.1 Distribution of Al atoms

To calculation of particle number, the proportion of metal elements on the receiving plate is measured by EDS. After ejection, the ratio of the metal elements reaching the receiving plate to the total number of metal elements ejected is calculated. The calculation is divided into two parts: (1) the number of particles of metal elements in the damaged area is determined, and (2) the number of particles of metal elements on the receiving plate is computed.

The number of particles of metal films ejected is N_1, which is expressed as:

$$N_1 = \frac{Ad\rho}{M} \cdot NA \tag{1}$$

where A is the damaged area after eruption on the surface of the metal films; d is metal film thickness; ρ is metal density; M is the molar mass of the metal; and $NA = 6.02\times10^{23}$.

The distribution area of the particles on the receiving plate is a circle. Starting from the center of the circle, along a certain direction of the radius, r is a fixed distance for the EDS test and the test areas S are all the same until the metal elements no longer appear. The result of the EDS test is the proportion of metal elements in several different test areas, which is $P_0\%$, $P_1\%$, $P_2\%,\cdots,P_n\%$. Furthermore, the number of particles in the ring area with a width of $\Delta r=r$ between the test points is the same, and this number is an arithmetic average of the density of the inner and outer rings.

The number of metal particles received on the receiving plate is N_2, which is expressed as:

$$N_2=\sum_{n=0}^{m}A_n\rho_n \tag{2}$$

where A_n is the nth ring area. A_0 is a circle with a radius of r and the center of the circle as the circle center, $A_0=\pi r^2, A_1=3\pi r^2, A_2=5\pi r^2,\cdots,A_n=(2n+1)\pi r^2$. The density of particles in the nth ring area is ρ_n:

$$\rho_n=\frac{N'\dfrac{P_n\%+P_{n+1}\%}{2}}{S}=\frac{3h\rho_{SiO_2}NA}{M_{SiO_2}}\cdot\frac{P_n\%+P_{n+1}\%}{2} \tag{3}$$

where N' is the total number of SiO_2 particles in the test area S and detection depth h. N' is approximated to the total number of particles.

Finally, the percentage of particles of metal elements received by the receiving plate η is expressed as:

$$\eta=\frac{N_2}{N_1}\times100\% \tag{4}$$

Then, the experimental results are calibrated by a series of standard samples. Using the aforementioned method to calculate the density of the number of particles of metal elements in the EDS test area, the number of particles in area S and depth h is approximately considered as the total number of test particles in the volume. However, the number of particles that EDS can detect plummets with the penetration depth. Therefore, the result needs to be corrected and calibrated. The steps for producing the standard sample are as follows:

(1) An Al film layer is coated with a thickness of d_0 (1 μm) on a fused silica substrate, marked as Class I sample;

(2) SiO_2 film layers of different thicknesses are coated onto Class I sample; the thicknesses of the SiO_2 film layers are integral multiples of 0.25 μm, marked as Class II samples;

(3) The Al ratio of Class I and Class II samples are measured by EDS, and the Al ratio of Class II samples are modified by using the measurement results of Class I sample;

(4) The thickness of the SiO_2 film layer and the modified Al ratio curve are plotted. When the Al ratio is 0, the thickness of the SiO_2 film layer is the penetration depth of EDS.

As shown in Fig.2, the EDS penetration depth is approximately 1.65 μm, and the total number of particles detected in Equation (3), $N'=\dfrac{3Sh\rho_{SiO_2}NA}{M_{SiO_2}}$ is fixed:

$$N'=\frac{3S\rho_{SiO_2}NA}{M_{SiO_2}}\int_0^{1.65}q\%\cdot\mathrm{d}h\approx\frac{3S\rho_{SiO_2}NA}{M_{SiO_2}}\sum_{n=1}^{7}0.25\times\frac{q_n\%+q_{n+1}\%}{2} \tag{5}$$

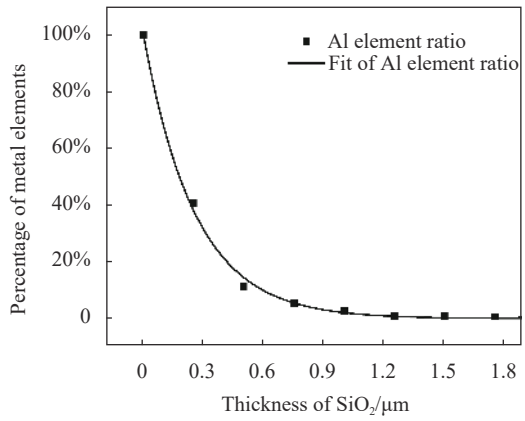

Fig.2 EDS measurements of 1 μm Al layer embedded in different depths of SiO_2 film. The horizontal coordinate is the thickness of the SiO_2 film layer, and the ordinate is the proportion of the quality of Al elements obtained by EDS. The measuring area is 50 μm×100 μm, the scanning time is 25 s, and the electron beam energy is 10 keV

where $q_n\%$ is the proportion of particles that can be detected by EDS under different thicknesses obtained from the experiments; and 0.25 μm is the film thickness step.

Equation (3) becomes:

$$\rho_n = \frac{N' \dfrac{p_n\% + P_{n+1}\%}{2}}{S} = \frac{3h'\rho_{SiO_2} NA}{M_{SiO_2}} \cdot \frac{p_n\% + P_{n+1}\%}{2} \quad (6)$$

where $h' = \sum_{n=1}^{7} 0.25 \times \dfrac{q_n\% + q_{n+1}\%}{2}$ can be defined as the equivalent penetration depth. The result of this calculation is $h' = 0.27$ μm. Actually, the results of EDS measurements of several metals are compared. The difference between the penetration depth and equivalent depth is not significant, which means that the penetration ability of specific X-ray signal to SiO_2 or fused silica is similar.

Under very high laser fluence, the metal layer and substrate of the Class I sample are damaged simultaneously, and most of the ejected particles are microns in size. The main component is SiO_2, which is mainly from the substrate itself, and the metal elements adhere to the SiO_2 particles. By contrast, under proper laser fluence, only the metal layer is damaged, and thermal evaporation ejects additional particles in atomic and ionic states. After a period of ejection and flight, the particles are deposited on the surface of the receiving plate. Through EDS measurements, the relative mass ratio of the metal elements can be obtained. The experimental results show that most of the metal elements are distributed within 2 mm on the receiving plate center which is placed 40 mm behind the sample, and the size of the film-peeling area is about 100–200 μm by 0.1 mm laser spot diameter.

2.2 Impact of environment and laser fluence

Differences in environments and laser fluences. Using Equations (1), (2), (4) and (6), the total number of atoms ejected by the Al film layer, the total number of atoms deposited on the receiving plate, and the deposited proportion can be determined. The distribution characteristics of Al elements on the receiving plate under different laser fluences in the atmospheric and vacuum environments are compared. As shown in Fig.3 and Tab.1, the thickness of Al film is 1 μm, which is coated by electron beam evaporation. The total number of ejected particles, the number of deposited particles, and the deposited proportion are roughly calculated. Figure 4 gives the damage morphology of Al film. Because of the stable film structure and the small internal stress, the damage morphology shows to be symmetrical.

Under the same laser fluences, the size of the

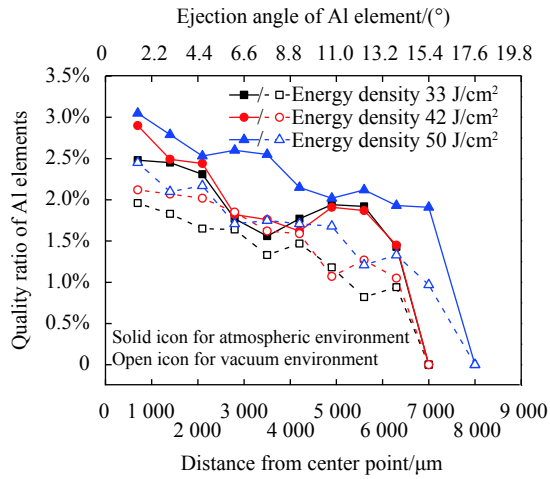

Fig.3 Distribution characteristics of Al particles in atmospheric and vacuum environments under different laser fluences

Tab.1 Number of Al particles received by the receiving plate under different conditions

Environment	Laser fluence/J·cm^{-2}	Total ejected particles	Total received particles	Percentage of reception
Atmosphere	33	$1.248\,1\times10^{16}$	$7.258\,3\times10^{15}$	58.16%
	42	$1.381\,4\times10^{16}$	$7.284\,7\times10^{15}$	52.73%
	50	$1.979\,8\times10^{16}$	$1.089\,2\times10^{16}$	55.01%
Vacuum	33	$1.201\,1\times10^{16}$	$4.892\,4\times10^{15}$	40.73%
	42	$1.444\,8\times10^{16}$	$5.654\,1\times10^{15}$	39.13%
	50	$2.019\,8\times10^{16}$	$7.375\,4\times10^{15}$	36.52%

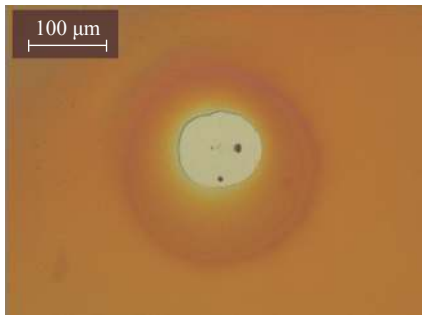

Fig.4 Damage morphology of Al film deposited by electron beam evaporation

damage of Al films in the atmospheric environment is close to that of the vacuum environment. In the atmospheric environment, about 50%-60% of the metal particles are usually received by the receiving plate. In the vacuum environment, this proportion is slightly lower. Because the oxygen-assisted combustion and reinforcement of plasma mass will not occur in the process of metal film damage, in which the plasma eruption will exert a secondary heating and kinetic energy transfer impact on metal atoms. Figure 5 shows the transient images of Al film in vacuum and atmospheric environment. The light of the detection area in the transient images is shielded, and a black region is formed. The transient eruption profile of the metal is related to the melting point, heat transfer coefficient, local temperature, flammability, and level of thermal evaporation. By comparison, it is easier to form strong plasma region in atmospheric environment. Moreover, in the atmospheric environment, the blocking effect of atmospheric molecules on the ejected atoms during flight is not significant.

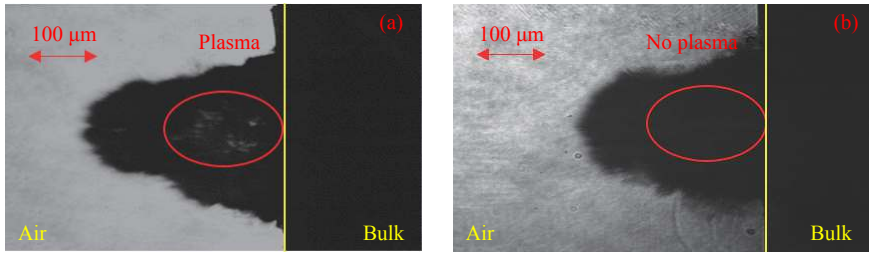

Fig.5 Transient ejection characteristics of Al film at 90 ns in different environments captured by pump-probe image technology. (a) Atmospheric environment; (b) Vacuum environment

2.3 Difference of different metal films

Compared with Al film, W film has a higher melting point (Al has a melting point of 660 ℃ and W has a melting point of 3410 ℃). The eruption process caused by thermal damage is affected by the high melting point and heat transfer of W film, which is significantly different from Al. In particular, the thermal stress required to cause damage of the same size and thermal evaporation effect is greater, and the laser energy is stronger.

Figure 6 shows the ejection transient images of 5 μm thick Al and W films in a vacuum environment at 90 ns delay. The ejection morphology is related to the metal characteristics, and the difference is very obvious. These characteristics also determine the distribution and proportion of the ejected atomic metal elements, as shown in Tab.2 and Fig.7. The receiving plate receives W

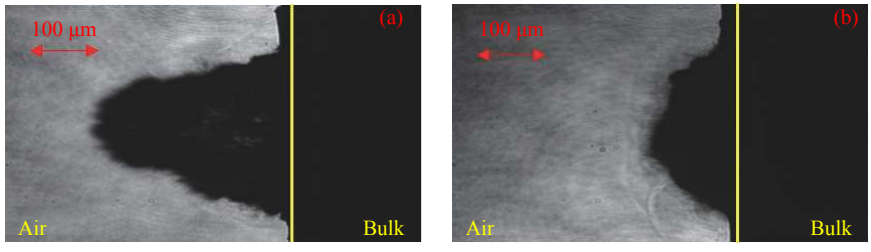

Fig.6 Transient image of (a) Al and (b) W film ejection in 90 ns under vacuum environment

Tab.2 Number of Al and W particles received by the receiving plate under different conditions

Environment	Fluence/J·cm^{-2}	Element	Total ejected particles	Total received particles	Percentage of reception
Atmosphere	33	Al	$1.394\,28\times10^{16}$	$9.043\,300\,08\times10^{15}$	64.86%
		W	$1.095\,06\times10^{16}$	$2.281\,009\,98\times10^{15}$	20.83%
Vacuum	33	Al	$1.344\,63\times10^{16}$	$7.805\,577\,15\times10^{15}$	58.05%
		W	$8.710\,92\times10^{15}$	$1.965\,183\,552\times10^{15}$	22.56%

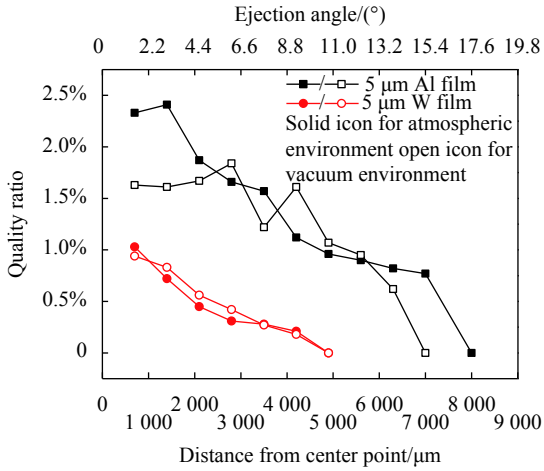

Fig.7 Distribution characteristics of Al and W element on the receiving plate in atmospheric and vacuum environments

significantly less than Al.

3 Conclusion

In addition, with the increase in laser fluence, the number of atoms received and the ejection angle increase, mainly concentrated in the range of 16°–20°, but the overall atomic reception ratio has not changed substantially or even slightly decreased due to loss effect.

Laser-induced thermal-mechanical damage causes the metal film layer to peel off. Only the metal layer is damaged, the metal is heated until it evaporates, forming an eruption of steam mass. It can be inferred that if the film structure is loose, uneven, too thick, or high stress inside, then residual debris is ejected. This phenomenon can substantially reduce the number of particles deposited on the receiving plate. Also, if the melting point is high and the metal is flammable, then the entire film layer evaporates incompletely both in the atmospheric and vacuum environments. A large number of molten particles will form uniform distribution, even in the molten state or as droplet-type debris, thereby reducing the number of particles deposited on the receiving plate.

In sum, by preparing a standard sample for EDS tests, the penetration depth of EDS is calibrated and the specific X-ray escape ratio at different depths is obtained. Then, the distribution of metal elements on the sample surface is approximately analyzed by EDS measurements. This method is necessary to estimate the number of atoms deposited after laser-induced thermal evaporation of a metal layer. Moreover, the number of deposited atoms of Al in the vacuum and atmospheric environments is calculated, and a detailed analysis and explanation are provided.

References:

[1] Guirlet R, Villegas D, Parisota T, et al. Anomalous transport of light and heavy impurities in Tore Supra sawtooth-free ohmic plasmas [J]. ***Nuclear Fusion***, 2009, 49(5): 055007.

[2] Zhang K, Cui Z Y, Sun P, et al. Investigation of impurity transport using laser blow-off technique in the HL-2A Ohmic and ECRH plasmas [J]. ***Chinese Physics B***, 2016, 25(6): 065202.

[3] Demos S G, Negres R A, Raman R N, et al. Relaxation dynamics of nanosecond laser superheated material in dielectrics [J]. ***Optica***, 2015, 2(8): 765-772.

[4] Salleo A, Taylor S T, Martin M C, et al. Laser-driven formation of a high-pressure phase in amorphous silica [J]. ***Nature Materials***, 2003, 2(12): 796-800.

[5] Papernov S, Schmid A W. Two mechanisms of crater formation in ultraviolet-pulsed-laser irradiated SiO_2 thin films with artificial defects [J]. ***Journal of Applied Physics***, 2005, 97(11): 114906.

[6] Rui S, Xiang M Z, Chen J, et al. Molecular dynamics simulation of shock induced ejection on fused silica surface [J]. ***Journal of Applied Physics***, 2014, 115(19): 27708.

[7] Natoli J Y, Gallais L, Akhouayri H, et al. Laser-induced damage of materials in bulk, thin-film, and liquid forms [J]. ***Applied Optics***, 2002, 41(16): 3156-3166.

[8] Manenkov A A. Fundamental mechanisms of laser-induced damage in optical materials: today's state of understanding and problems [J]. ***Optical Engineering***, 2014, 53(1): 010901.

[9] Ma B, Zhang Y Y, Ma H P, et al. Highly sensitive compact refractive index sensor based on phase-shifted sidewall Bragg gratings in slot waveguide [J]. ***Applied Optics***, 2014, 53(1): 96-103.

[10] Lu M L, Ma B, Zhan G D, et al. Effect of etching on the laser-induced damage properties of artificial defects under 1064 nm laser irradiation [J]. ***Optical Engineering***, 2014, 53(12): 122505.

[11] Cheng X B, Zhang J L, Ding T, et al. The effect of an electric field on the thermomechanical damage of nodular defects in dielectric multilayer coatings irradiated by nanosecond laser pulses [J]. ***Light: Science & Applications***, 2013, 2(6): e80.

[12] Gallais L, Natoli J Y, Amra C. Statistical study of single and multiple pulse laser-induced damage in glasses [J]. ***Optics Express***, 2002, 10(25): 1465-1474.

[13] Bude J, Miller P, Baxamusa S, et al. High fluence laser damage precursors and their mitigation in fused silica [J]. ***Optics Express***, 2014, 22(5): 5839-5851.

[14] Raman R N, Negres R A, Demos S G. Kinetics of ejected particles during breakdown in fused silica by nanosecond laser pulses [J]. ***Applied Physics Letter***, 2011, 98(5): 051901.

[15] Demos S G, Negres R A, Raman R N, et al. Material response during nanosecond laser induced breakdown inside of the exit surface of fused silica [J]. ***Laser & Photonics Reviews***, 2013, 7(3): 444-452.

[16] Zhang N, Zhu X, Yang J, et al. Time-resolved shadowgraphs of material ejection in intense femtosecond laser ablation of aluminum [J]. ***Physical Review Letters***, 2007, 99(16): 167602.

[17] Goldstein J I, Newbury D E, Michael J R, et al. Scanning Electron Microscopy and X-Ray Microanalysis [M]. US: Springer, 2018.

[18] Park J H, Seo J, Park S, et al. Efficient $CH_3NH_3PbI_3$ perovskite solar cells employing nanostructured p-type NiO electrode formed by a pulsed laser deposition [J]. ***Advanced Materials***, 2015, 27(27): 4013-4019.